Formation kinetics and mechanism of ozone and secondary organic aerosols from photochemical oxidation of different aromatic hydrocarbons: dependence on NOx and organic substituent

Hao Luo[1,2,★], Jiangyao Chen[1,2,★], Guiying Li [1,2], and Taicheng An[1,2]

[1]Guangdong Key Laboratory of Environmental Catalysis and Health Risk Control, Guangdong-Hong Kong-Macao Joint Laboratory for Contaminants Exposure and Health, Institute of Environmental Health and Pollution control, Guangdong University of Technology, Guangzhou 510006, China
[2]Guangzhou Key Laboratory of Environmental Catalysis and Pollution Control, Key Laboratory of City Cluster Environmental Safety and Green Development, School of Environmental Science and Engineering, Guangdong University of Technology, Guangzhou 510006, China

★ These authors contributed equally to this work.

Correspondence to: Taicheng An (antc99@gdut.edu.cn)

Abstract. Aromatic hydrocarbons (AHs) contribute significantly to ozone and secondary organic aerosol (SOA) formation in atmosphere, but formation mechanisms are still unclear. Herein, photochemical oxidation of nine AHs was investigated in chamber. Only small amount of ozone was produced from direct photochemical oxidation of AHs, while fewer AH substituent number resulted in higher concentrated ozone. Addition of NOx increased ozone and SOA production. Synergetic effect of accelerated NO_2 conversion and NO reaction with AHs boosted ozone and volatile intermediate formation. Promoting AH concentration in VOC/NOx ratio further increased formation rates and concentrations of both ozone and SOA. Additionally, ozone formation was enhanced with increasing AH's substituent number but negligibly affected by their substituent position. Differently, SOA yield decreased with increased substituent number of AHs, but increased with ortho methyl group substituted AHs. Model fitting and intermediate consistently confirmed that increasing substituent number on phenyl ring inhibited generating dicarbonyl intermediates, which however were preferentially produced from oxidation of ortho methyl group substituted AHs, resulting in different changing trend of SOA yield. The restrained oligomerization by increased substituent number was another main cause for decreased SOA yield. These results are helpful to understand photochemical transformation of AHs to secondary pollutants in real atmosphere.

1 Introduction

As an abundant group of volatile organic compounds (VOCs), aromatic hydrocarbons (AHs) are important precursors of ozone (O_3) and secondary organic aerosols (SOA) in atmospheric environment (Peng et al., 2017;Tong et al., 2020), directly or indirectly threatening air quality and public health (Henze et al., 2008;Lane et al., 2008;Yang et al., 2016). Atmospheric AHs mainly come from anthropogenic sources, such as industrial emission and motor vehicle emissions (Luo et al.,

2020a;Sun et al., 2018;Chen et al., 2020;An et al., 2014;He et al., 2015), and these emitted AHs are commonly composed of single phenyl ring with less than four methyl groups (e.g., toluene, xylene) or ethyl groups (e.g., ethylbenzene) (Han et al., 2019;Hu et al., 2015;Chen et al., 2019). It is also found that photochemical oxidation of these AHs are sensitive to reaction conditions (e.g., VOC/NO_x ratio (Odum et al., 1996;Metzger et al., 2008;Bloss et al., 2005a;Carter and Heo, 2013)), ultimately influencing the formation kinetics and mechanism of O_3 and SOA from AH oxidation (Borrás and Tortajada-Genaro, 2012;Sato et al., 2010;Cocker III et al., 2001;Ji et al., 2017;Jia and Xu, 2018).

Previous experimental simulation studies have confirmed that relatively high VOC/NO_x ratio had an inhibitory effect on SOA productivity (Wang et al., 2015), while VOC/NO_x ratio might also influence O_3 formation (Wang et al., 2016). From field observation, the actual ratio of VOC/NO_x in the atmosphere is always changed with the variation of the seasons (Geng et al., 2008;Zou et al., 2015;Li et al., 2013;Seinfeld, 1989). Nevertheless, although it is of important environmental significance, the studies about influence of VOC/NO_x ratio on photochemical oxidation of AHs to form O_3 and SOA are mostly focused on the varied NO_x concentration. The effects of AH content as well as substitute groups of AHs to the formation kinetics and mechanism of O_3 and SOA are still unconcerned. Therefore, in view of the complexity of the real atmosphere, it is very necessary to effectively simulate atmospheric photochemical reactions at different VOC/NO_x ratios in laboratory smog chamber and explore the formation kinetics and mechanism of O_3 and SOA from AHs at different concentrations.

Usually, OH-initiated reactions have been confirmed to dominate in AH photochemical oxidation (Ji et al., 2018), in which the reaction rate constant increases with increased substituent number of AHs (Atkinson and Arey, 2003;Aschmann et al., 2013;Glasson and Tuesday, 1970). The important role of substituent position has also been observed in the OH-initiated alkane and alkene oxidation (Atkinson, 2007;Ziemann, 2011). All these previous studies inspire us that the influence of substituent, including number and position, on the photochemical transformation of AHs to O_3 and SOA cannot be ignored. However, although both O_3 and SOA generated from different AHs have been studied in laboratory smog chamber simulations, the role of AH's substituent to the formation kinetics and mechanism of O_3 and SOA as well as their relationship with the oxidation intermediates have not been systematically investigated and established.

In this work, nine AHs with different substituent number and position (e.g., benzene, toluene, ethylbenzene, m-xylene, o-xylene, p-xylene, 123-trimethylbenzene, 124-trimethylbenzene, 135-trimethylbenzene) were chosen to study their photochemical oxidation behaviour in an indoor smog chamber system, to compare the formation activity in O_3 and SOA. The influences of NO_x, AH concentration and AH substituent on the formation kinetics of O_3 and SOA were studied in detail. All volatile intermediates were qualitatively and quantitatively online analysed to propose their potential contribution to the formation of O_3 and SOA. The relationship between AH structure, intermediate, and production of O_3 and SOA were established to reveal the transformation mechanism of AHs to O_3 and SOA. The results of this work will further elucidate the photochemical behaviour of AHs in the atmosphere and provide reliable experimental data for modelling and prediction in the future.

2 Experimental

2.1. Photochemical oxidation experiment

All experiments were conducted in GDUT-DRC dual-reactor chamber with two 2 m^3 pillow-shaped reactors and the detail description of the reactor was reported in our early work (Luo et al., 2020b). The experimental relative humidity (RH) and temperature was set as < 5% and around 303 ± 1 K, respectively. No inorganic seed aerosol was supplied in this work. A total of 60 black lamps (40 W, F40BL, GE, USA) were equipped to provide UV light source, and the light intensity in the dual-reactor were determined to be 0.161 min^{-1} (left) and 0.169 min^{-1} (right) by using the NO_2 photolysis rate constant (Luo et al., 2020b). The centre of the UV lamp wavelength was 360 nm.

Nine AHs (benzene, 99.5%; toluene, 99.0%; ethylbenzene, 99.8%; m-xylene, 99.0%; o-xylene, 99.0%; p-xylene, 99.0%; 1,2,3-trimethylbenzene (123-TMB), 90.0%; 1,2,4-trimethylbenzene (124-TMB), 98.0%; 1,3,5-trimethylbenzene (135-TMB), 97.0%) purchased from Aladdin Industrial Co., Ltd. (USA) and certain amount of NO_2 were directly injected into the reactor to conduct the photochemical oxidation experiments. Before turning on the light, all AHs and NO_2 were injected with the background gas flow and adjusted to stable for one hour. Typical experimental conditions (e.g., concentrations of AHs and NOx, VOC/NOx ratio, RH and temperature) of this study for nine AHs are supplied in Supporting Information (SI) as Table S1.

2.2. Organic gas measurement

The concentrations of AHs and their oxidation products were all measured online using proton-transfer reaction time-of-flight mass spectrometry (PTR-ToF-MS, Ionicon Analytik Inc., Austria). In the setting model, all gaseous organics with proton affinity greater than H_2O including AHs, hydrocarbons, acids and carbonyl groups, were all measured quantitatively and qualitatively. By processing software TOF-DAQ (Tofwerk AG, Switzerland), it recorded the material with m/z≤240 and the original signal strength was converted into ppb concentration by formula (Lindinger et al., 1998). Before sampling and measurement, PTR-ToF-MS was calibrated and the instrument was calibrated once a week during all measurement period (Han et al., 2019). The detection limit of PTR-ToF-MS was < 20 ppt for m/z 79 and < 10 ppt for m/z 181 within averaged over 1 min). Detailed parameters of the instrument and the yield calculation formula of products were given in SI.

2.3. Inorganic gas measurement

The real-time concentrations of NO, NO_2, and NO_x were all spontaneously monitored with NO_x analyzer (Model 42i, Thermo Scientific Inc., USA), and the real-time concentration of O_3 was monitored with O_3 analyzer (Model 49i, Thermo Scientific Inc., USA). The detection limits of NOx and O_3 analyzers were < 0.4 ppb within averaged over 1 min and 0.5 ppb, respectively. All devices were calibrated weekly using gas calibrator (Model 146i, Thermo Scientific Inc., USA).

2.4. Particle measurement

Particle size distribution was measured by scanning mobility particle sizer spectrometer (SMPS, TSI Inc., USA) equipped with electrostatic classifiers (EC, Model 3082, TSI Inc., USA) and long differential mobility analyzer (DMA) (Model 3081, TSI Inc., USA), or an optional nano DMA (Model 3085, TSI Inc., USA) and a condensation particle counter (CPC, Model 3776, TSI Inc., USA). The velocities of sheath gas and aerosol flows were set at 3.0 and 0.3 L min^{-1}, respectively. Under this setting, the particle size range was observed from 13.8 to 723.4 nm. The yield calculation formula of SOA was given in SI.

3 Results and discussion

3.1 Formation kinetics and mechanism of O_3 and SOA without NO_x

The directly photochemical oxidation of nine AHs was first conducted to evaluate the formation potential of O_3 and SOA. No SOA was detected within 480 min's reaction duration. The O_3 concentration increased steadily from 0 to 16 ppb for 135-TMB and 28 ppb for ethylbenzene within 420 min (Fig. 1a). The peak concentration of O_3 for these nine AHs followed the trend of (ethylbenzene, toluene, benzene, 23 − 28 ppb) > (m-, o-, p-xylene, 18 − 21 ppb) > (123-, 124-, 135-TMB, 16 − 20 ppb). Clearly, fewer number of AH substituent resulted in generation of higher concentrated O_3. This may be because that the substituent number of AHs determined their reactivity, while the reaction rate constants with •OH could be applied to evaluate the reactivity. Previous studies indicated that the rate constants of AHs with •OH was found obeying the order of toluene $(5.61 \pm 0.08) \times 10^{-12}$ cm^3 $molecule^{-1}$ s^{-1} < xylene $(7.4 - 14) \times 10^{-12}$ cm^3 $molecule^{-1}$ s^{-1} < TMB $(14 - 31) \times 10^{-12}$ cm^3 $molecule^{-1}$ s^{-1} at 304 ± 1 K (Doyle et al., 1975;Anderson and Hites, 1996). Combining with our results herewith, it is solidly concluded that AHs with fewer substituent number showed lower reactivity, and then resulting in higher concentrated O_3 formation.

Furthermore, to figure out the formation mechanism of O_3 from direct AH oxidation, the correspondingly volatile intermediates were also monitored. Toluene was taken as an example to illustrate the concentration variation of volatile intermediates. As Fig. 1b shows, with decrease of toluene's concentration from 996 to 944.5 ppb, the concentrations of nine intermediates increased at different degrees. The concentrations of m/z = 45 (m45, acetaldehyde), m/z = 47 (m47, formic acid) and m/z = 61 (m61, acetic acid or glycolaldehyde) increased faster than others, and peaked at 5 − 9 ppb within 450 min, indicating easily oxidation of toluene to small molecular carbonyl products. The peak concentration of m/z = 99 (m99, 3-methyl-2(5H)-furanone or 4-keto-2-pentenal) reached 4.2 ppb, while the productions of m/z = 31 (m31, formaldehyde), m/z = 59 (m59, glyoxal), m/z = 73 (m73, methylglyoxal) were at the same level (ca. 2.4 ppb). The concentrations of some intermediates including m/z = 85 (m85, 2-butenedial), m/z = 87 (m87, butanedione) and m/z = 111 (m111, hexa-2,4-dienedial) were lower than 0.8 ppb within 450 min's reaction duration. Similar variation trends of volatile intermediates were observed from other eight AHs (Fig. S1).

It was worth mentioning that most of above intermediates were well-known precursors of O_3 and SOA (Li et al., 2016;Ji et al., 2017;Nishino et al., 2010). However, the formation of SOA was not observed in this study. Two reasons might be involved. Since this study was carried out at low RH (< 5%) and without seed particles, no SOA precursor oligomers existed. Furthermore, the concentrations of produced intermediates were too low to trigger the initial nucleation reaction and then generate SOA under low RH condition. Therefore, SOA formation could not be observed in the NO_x−free photochemical oxidation of these nine AHs. In general, tropospheric O_3 was mainly from NO_2 photolysis and the existence of AHs could enhance O_3 formation. However, when the absent of NO_x in this study, the low concentrated O_3 was observed from AH photochemical oxidation. The possible contributors of these O_3 might be intermediates such as carbonyl compounds. In all, our results indicated that direct photochemical transformation of AHs to O_3 actually occurred and should be taken into consideration in the atmospheric environment.

3.2. Formation kinetics and mechanism of O_3 in the presence of NO_x

To further explore the role of NO_x in O_3 formation during photochemical oxidation of AHs, about 160 ± 10 ppb of NO_2 was added into the reactor. The concentration of NO_2 was selected based on previous works (Luo et al., 2019; Chen et al., 2018). Under this condition, the generated O_3 was found significantly increasing and the O_3 peak concentrations ranged from 230 to 440 ppb within 100 to 250 min (Fig. 2). All these data were about 200 − 400 ppb higher than those obtained in the absence of NO_x (Fig. 1a), indicating quick enhancement of NO_x to O_3 formation. In this work, the added NO_2 was firstly photolyzed under 360 nm's light irradiation to from NO and $O(^3P)$ (Eq. 1). Then, the latter was oxidized to form O_3 (Eq. 2), which further reacted with NO to form NO_2 (Eq. 3). Meanwhile, AHs were photochemically oxidized to form RO_2 and HO_2, both of which then reacted with NO to form NO_2 (Eqs. 4 and 5). Clearly, the presence of AHs could compete with O_3 for the NO reaction and reduce the consumption of O_3. The synergetic effect of direct NO_2 conversion and AH's competition reaction led to the boosting formation of O_3 in the presence of both AHs and NO_x.

$$NO_2 + h\nu\ (\lambda = 360\ nm) \rightarrow NO + O(^3P) \quad (1)$$

$$O(^3P) + O_2 \rightarrow O_3 \quad (2)$$

$$NO + O_3 \rightarrow NO_2 \quad (3)$$

$$RO_2 + NO \rightarrow NO_2 + RO \quad (4)$$

$$HO_2 + NO \rightarrow NO_2 + {}^{\bullet}OH \quad (5)$$

Furthermore, the effect of AH content on the O_3 formation in the presence of NO_x (e.g., VOC/NO_x ratio) was investigated. Here, the concentration of NO_x was maintained constantly and that of AH was gradually increased. For toluene (Fig. 3a), O_3 peak concentration of 250 ppb was achieved after reaction for 420 min under VOC/NO_x ratio of 2.47. When increasing VOC/NO_x ratio to 6.29, the time needed achieving higher peak O_3 concentration of 280 ppb was shortened to be 150 min. All these data confirmed that O_3 formation rate and concentration were both accelerated with increased AH

concentration. Similar results of shorter reaction time leading to higher O_3 concentration were observed for the rest AHs (Fig. S2). Increasing AH concentration would result in the enhanced formation of RO_2 and HO_2, both of which reacted with NO to save the O_3 consumption. Meanwhile, the photolysis of NO_2 to form NO and then O_3 was also accelerated. Both of these reasons were responsible for the fast-enhanced formation of O_3 with the increased AH concentration in VOC/NO_x ratio.

To study the effect of AH's substituent on O_3 formation, the O_3 peak concentrations of nine AHs obtained at the same VOC/NO_x ratio were compared. As Fig. 3b shows, the O_3 peak concentrations of nine AHs followed the order of TMB (366.4 − 431.2 ppb) > xylene (290.6 − 365.7 ppb) > toluene and ethylbenzene (246.7 − 291.7 ppb) > benzene (187.3 − 231.2 ppb). Clearly, the O_3 peak value was positively correlated with the number of AH's substituent, suggesting AHs with more substituent possessed higher O_3 production potential at the same VOC/NO_x ratio. In previous studies, O_3 concentrations from AH oxidation with the presence of NO_x were reported as follows: 160 − 300 ppb for toluene, 400 ppb for m-xylene, and 340 − 470 ppb for 123-TMB (Luo et al., 2019;Li et al., 2018;Xu et al., 2015). However, these studies only focused on one or several AHs, and the relationship between AH substituent and O_3 formation was still not understood. Meanwhile, the VOC/NOx ratio ranging from 1.0 to 13.0 was selected to its effect to O_3 formation. The range of VOC/NO_x ratio in above researches was close to that in our study (Table S2). Then, our results of O_3 concentration were comparable to those in the previous studies under similar range of VOC/NO_x ratio. Furthermore, the results obtained in this study clearly confirmed that increasing substituent number of AH correspondingly increased O_3 concentration. It was also noticed that the O_3 peak concentrations of xylene or TMB isomers were in the same range, suggesting negligible effect of substituent position of AHs to their O_3 formation.

3.3. Accelerated formation of SOA in the presence of NO_x

Besides O_3, the effect of AH concentration on formation kinetics of SOA with the presence of NOx was also investigated. As Fig. 4 shows, from photochemical oxidation of toluene, the peak number concentration of SOA increased from 2.0×10^4 to 5.5×10^4 particle cm^{-3} with increase of VOC/NO_x ratio from 2.37 to 5.58. The time achieving above concentration was shortened from 250 to 120 min, while the median particle size range also increased from 300 − 400 to 400 − 500 nm. Similar results of shorter time leading to higher concentration and larger particle size for SOA were observed for other eight AHs with the increasing VOC/NO_x ratio (Figs. S3-S10).

Previous studies reported the enhanced SOA yield by increased NO_x concentration (Zhao et al., 2018;Hurley et al., 2001;Song et al., 2007;Sarrafzadeh et al., 2016). This was because that NO_x mainly influenced the distribution of oxidation products by affecting the RO_2 reaction equilibrium, where RO_2 easily converted to low-volatile ROOH or ROOR and thus resulted in the nucleation of new particles (Sarrafzadeh et al., 2016). However, in this study, we kept the NO_x concentration unchanged, and modified the initial concentration of AHs. The increased AHs could lead to promoted RO_2 formation, resulting in more low-volatile products formation. The accumulation of low-volatile products promoted the nucleation of particulate matter and finally increased the yield of SOA.

The particle number and mass concentrations of SOA generated from nine AHs were further compared to evaluate the effect of AH's substituent on the SOA formation. The particle number concentration of SOA was obtained at the endpoint of each reaction. With the increase of substituent number, the number concentration of SOA decreases (e.g., from 6.9×10^3 particle m^{-3} for 135-TMB to 7.8×10^4 particle m^{-3} for toluene) (Fig. 5a). With the progress of the reaction, the mass concentration of SOA increased, and the increase of substituent number shortened the time achieving the peak mass concentration (Fig. 5b). These results revealed that the increase of substituent number of AHs increased SOA's mass concentration but decreased its particle number. AHs with different substituent position also showed different SOA formation characteristics. For xylene, the peak mass concentration of o-xylene (88.6 μg m^{-3}) was higher than that of m-xylene and p-xylene, while the peak mass concentration of 123-TMB (82.0 μg m^{-3}) was significantly higher than those of 124-TMB (31.8 μg m^{-3}) and 135-TMB (27.6 μg m^{-3}) (Fig. 5b). These phenomena indicated that xylene and TMB with ortho methyl substituent facilitated the SOA formation. Further, the ortho methyl group of isomers (e.g. o-xylene, 123-TMB) could more thoroughly be oxidized, producing more particles (Sato et al., 2010).

It has also been reported that seed particles (e.g., NaCl) and highly relative humidity (up to 90%) can significantly increase the yield of SOA (Wang et al., 2016;Luo et al., 2019;Jia and Xu, 2018). However, in this study, the maximum SOA yield of 25% (Fig. S11) was produced with increasing AH concentration, which was consistent with that from previous researches (Sato et al., 2012;Li et al., 2016;Song et al., 2007;Odum et al., 1997). Further considering the oxidation conditions of low RH (less than 5%) and seedless particles in this study, our results indicated that AH concentration should also be paid much attention to SOA formation although the addition of NO_x, seed particles and high RH are all very important.

To further investigate the effect of AH's substituent on SOA yield, a two-product semi-empirical model was employed. As Fig. S12 shows, the model well fitted the SOA yield of nine AHs and the correspondingly fitting parameters are listed in Table 1. Similarly, high-volatile components were assumed from the photochemical oxidation of AHs and same $K_{om,2}$ of 0.005 m^3 μg^{-1} was assigned. As seen from the table, benzene (0.242 m^3 μg^{-1}), toluene (0.162 m^3 μg^{-1}) and ethylbenzene (0.422 m^3 μg^{-1}) showed higher α_2 than that of xylenes (e.g., 0.086 m^3 μg^{-1} for m-xylene) and TMBs (e.g., 0.082 m^3 μg^{-1} for 123-TMB), indicating the production of more high-volatile products from AHs with less number of substituent. Meanwhile, benzene (0.022 m^3 μg^{-1}), toluene (0.027 m^3 μg^{-1}) and ethylbenzene (0.023 m^3 μg^{-1}) displayed lower $K_{om,1}$ in comparison with xylenes (e.g., 0.074 m^3 μg^{-1} for p-xylene) and TMBs (e.g., 0.085 m^3 μg^{-1} for 135-TMB), and the corresponding α_1 decreased with increasing substituent number. All these results demonstrated that the increase of substituent number on phenyl ring inhibited the generation of low-volatile products, thus reducing the generation of SOA particles, finally leading to the decrease of SOA yield. The result also indicated that the oxidation degree became lower and lower for AHs with increased substituent number, since the oxidation of methyl carbon was more difficult than that of carbon of phenyl ring. Li et al. reported similar phenomenon at early time,(Li et al., 2016) and is consistent with our results. However, they did not further investigate the relationship of isomer AH with the SOA yield.

In the present study, SOA yield of o-xylene was found higher than that of m-xylene and p-xylene, consistent with the SOA number and mass results. The fitting results showed that the $K_{om,1}$ of o-xylene (0.024 m^3 μg^{-1}) was much lower than that of m-xylene (0.057 m^3 μg^{-1}) and p-xylene (0.074 m^3 μg^{-1}), indicating the production of more low-volatile products from o-xylene. Similarly, 123-TMB showed the highest SOA yield and lowest $K_{om,1}$ among three TMBs. These results further confirmed that AHs with ortho methyl substituent favoured the yield of SOA. This might be because that these AHs were more susceptible to be oxidized, formed ring-opening products and finally produced more RO_2 than other isomers. Some previous studies have also obtained consistent results (Zhou et al., 2011;Song et al., 2007). In addition, ethylbenzene was also isomeric to xylene, and its SOA yield was higher than that of xylenes. Recent studies have found that the SOA yield during the oxidation of alkanes and alkenes by ·OH increased with the carbon chain length (Lim and Ziemann, 2009;Tkacik et al., 2012). Obviously, the length of carbon chain also affected the oxidation degree of AHs. Then, the longer ethyl group led to a higher degree of photochemical oxidation for ethylbenzene than xylenes, promoting the formation of more SOA precursors and finally higher SOA yield.

3.4. Enhanced formation mechanism of SOA with NO_x

In order to further reveal the enhanced formation mechanism of SOA from the oxidation of AHs with the presence of NOx, the corresponding volatile intermediates were all identified, and quantified comparably. As Fig. 6a shows, with gradual decrease of toluene concentration, the concentrations of small molecule carbonyl products, such as m31, m45, m47 and m61, quickly increased to 16.0, 45.3, 31.0 and 17.0 ppb within 200 min. Acetaldehyde showed the highest concentration, which was by far higher than that obtained without NO_x (9 ppb). Followed one were m85, m87 and m111 with the peak concentration below 2.8 ppb. The increase of concentration of m59, m73 and m99 began to slow down after 120 min, and this trend was consistent with the trend of SOA formation (Fig. 5b). Similar variation trend of volatile intermediates for other AHs was also measured (Fig. S13). All these results demonstrated that there was a specific window period, and the intermediates in the gaseous phase were transformed into the particulate phase. The significant increase of SOA occurred after breaking through the window period.

Further comparison of volatile intermediates during photochemical oxidation of AHs with different VOC/NO_x ratio was also carried out. For toluene oxidation (Fig. 6b and 6c), the concentrations of all intermediates increased with the increase of VOC/NO_x ratio. The carbonyl intermediates such as m59 and m73 were believed to be playing important role in the photochemical oxidation of AHs to form SOA (Li et al., 2016;Ji et al., 2017;Nishino et al., 2010). Bloss et al. also found glyoxal and methylglyoxal produced from toluene photochemical oxidation as the main precursor of SOA (Bloss et al., 2005b). In previous studies, the maximum yield of glyoxal and methylglyoxal were obtained as 20% and 17% during toluene photochemical oxidation (Baltaretu et al., 2009;Volkamer et al., 2001;Nishino et al., 2010), which was lower than that of the present study (24% in Fig. 6c). Meanwhile, the yields of glyoxal and methylglyoxal during photochemical oxidation of toluene, xylenes and TMBs increased with increasing AH concentration. Therefore, the increase of AH content in reaction system promoted the photochemical oxidation of AHs to produce more volatile carbonyl intermediates, finally leading to

higher SOA yield in this study. Moreover, the yield of m59 and m73 from benzene photochemical oxidation was found the lowest among all AHs (Figs. 6b, 6c and S14-S22), indicating that the presence of branch chain on phenyl ring did not favour the production of unsaturated carbonyl compounds. This was because that increasing methyl group number of AHs weakened their oxidation reactivity, resulting in the inhibition of ring-opening reaction (Li et al., 2016). Further, the formation of glyoxal and methylglyoxal from RO_2 were also subsequently suppressed. Furthermore, the yields of m85 from AHs containing ortho methyl group (e.g., o-xylene, 123-TMB and 124-TMB) were found higher than that of their isomers, due to that ortho methyl groups of phenyl ring preferred to ring opening and then generation of ketone products (Li et al., 2016).

Based on the above results, the possible photochemical oxidation mechanism from AH to SOA were proposed. Toluene was selected as an example. As Fig. 7 shows, phenyl ring of toluene firstly reacted with ·OH to produce cresol (Ziemann, 2011;Atkinson, 2007), and then further oxidized to form an intermediate which could occur ring-opening reaction or react with HO_2 radicals to form bicyclic peroxide compounds. The latter has been suggested as important SOA precursor from AH photochemical oxidation (Song et al., 2005;Wyche et al., 2009;Nakao et al., 2011;Johnson et al., 2005). The ring-opening intermediates were consisted of saturated and unsaturated dicarbonyl compounds (Jang and Kamens, 2001;Birdsall and Elrod, 2011). However, the possibility of these dicarbonyl intermediates directly partitioning into the particulate phase was very small (Jang and Kamens, 2001), but they could oligomerize to form low-volatility compounds (Forstner et al., 1997;Jang and Kamens, 2001). The oligomerization was an important pathway for SOA formation from AH photochemical oxidation (Sato et al., 2012;Li et al., 2016;Hu et al., 2007). In our study, the detection of m85 and m99 proved the formation of ring-opening products. These unsaturated 1,4-dicarbonyls were observed to form small cyclic furanone compounds (Jang and Kamens, 2001;Bloss et al., 2005b). Therefore, the ring-opening products with saturated or unsaturated dicarbonyl groups finally transformed into SOA through oligomerization process.

As mentioned above, with the increase of the substituent number on AHs, the yield of SOA decreased. The enhanced ring-opening products and restrained oligomerization reactions by the increased methyl group number were supposed to be the main cause. The methyl group was found to stabilize the ring-opening radicals (Ziemann, 2011). When phenyl ring contained methyl group, the oxidation pathway was prone to ring-opening. The concentrations of m87 and m111 increased with the methyl group number increasing (Fig. S23), meaning that these two intermediates were dominant in the ring-opening products. However, they could not oligomerize to further partition into SOA formation (Fig. 7). Both non-cyclic dicarbonyls and cyclic compounds formed by unsaturated dicarbonyls were deemed to have small probability to oligomerize (Li et al., 2016;Kalberer et al., 2004). In previous study, no m85 and m111 were detected in particulate phase SOA under 300 ± 1 K and dry conditions (RH < 0.1%) in the absence of inorganic seed aerosol (Li et al., 2016). However, m85 was measured in gas phase of this study, indicating that it was not the precursor of SOA for the oligomerization reaction. The presence of methyl groups would inhibit the oligomerization to prevent the formation of ring compounds by unsaturated dicarbonyl groups and finally decrease SOA formation.

4 Conclusions

In this study, no SOA formation was observed from direct photochemical oxidation of AHs, while a small amount of O_3 was produced without NO_x addition. The presence of NO_x significantly increased the productions of O_3 and SOA, due to synergetic effect of accelerated NO_2 conversion and AH reaction with NO as well as enhanced formation of volatile intermediates. Further increased formation of both O_3 and SOA were observed by promoted AH concentration. In addition, increase of AH's substituent number could enhance O_3 formation, but decrease SOA yield. The ortho methyl group substituted AHs exhibited higher SOA yield. The preferential formation of variation of dicarbonyl intermediates and restrained oligomerization reaction were responsible for above differences. These results showed more clear understanding of the effect of NO_x and organic molecule structures on photochemical oxidation of AHs to form O_3 and SOA, which could provide solidly experimental basis for studying the transformation of AHs to secondary pollutants in the real atmospheric environment.

Supplement. The supplement related to this article is available online at:

Author contributions. TA designed research. HL and JC conducted experiments. HL, JC and GL analyzed data. HL prepared the manuscript with contributions from all co-authors.

Competing interests. The authors declare that they have no conflict of interest.

Financial support. This work was supported by the National Natural Science Foundation of China (42020104001), Local Innovative and Research Team Project of Guangdong Pearl River Talents Program (2017BT01Z032), Guangdong Provincial Key Research and Development Program (2019B110206002) and National Key R&D Program of China (2019YFC0214402).

References

An, T. C., Huang, Y., Li, G. Y., He, Z. G., Chen, J. Y., and Zhang, C. S.: Pollution profiles and health risk assessment of VOCs emitted during e-waste dismantling processes associated with different dismantling methods, Environ. Int., 73, 186-194, 10.1016/j.envint.2014.07.019, 2014.

Anderson, P. N., and Hites, R. A.: OH radical reactions: the major removal pathway for polychlorinated biphenyls from the atmosphere, Environ. Sci. Technol., 30, 1756-1763, 1996.

Aschmann, S. M., Arey, J., and Atkinson, R.: Rate constants for the reactions of OH radicals with 1,2,4,5-tetramethylbenzene, pentamethylbenzene, 2,4,5-trimethylbenzaldehyde, 2,4,5-trimethylphenol, and 3-methyl-3-hexene-2,5-dione and products of OH + 1,2,4,5-tetramethylbenzene, J. Phys. Chem. A, 117, 2556-2568, 10.1021/jp400323n, 2013.

Atkinson, R., and Arey, J.: Gas-phase tropospheric chemistry of biogenic volatile organic compounds: a review, Atmos. Environ., 37, 197-

219, 10.1016/s1352-2310(03)00391-1, 2003.

Atkinson, R.: Rate constants for the atmospheric reactions of alkoxy radicals: An updated estimation method, Atmos. Environ., 41, 8468-8485, 10.1016/j.atmosenv.2007.07.002, 2007.

Baltaretu, C. O., Lichtman, E. I., Hadler, A. B., and Elrod, M. J.: Primary atmospheric oxidation mechanism for toluene, J. Phys. Chem. A, 113, 221-230, 2009.

Birdsall, A. W., and Elrod, M. J.: Comprehensive NO-dependent study of the products of the oxidation of atmospherically relevant aromatic compounds, J. Phys. Chem. A, 115, 5397-5407, 10.1021/jp2010327, 2011.

Bloss, C., Wagner, V., Bonzanini, A., Jenkin, M. E., Wirtz, K., Martin-Reviejo, M., and Pilling, M. J.: Evaluation of detailed aromatic mechanisms (MCMv3 and MCMv3.1) against environmental chamber data, Atmos. Chem. Phys., 5, 623-639, DOI 10.5194/acp-5-623-2005, 2005a.

Bloss, C., Wagner, V., Jenkin, M. E., Volkamer, R., Bloss, W. J., Lee, J. D., Heard, D. E., Wirtz, K., Martin-Reviejo, M., Rea, G., Wenger, J. C., and Pilling, M. J.: Development of a detailed chemical mechanism (MCMv3.1) for the atmospheric oxidation of aromatic hydrocarbons, Atmos. Chem. Phys., 5, 641-664, DOI 10.5194/acp-5-641-2005, 2005b.

Borrás, E., and Tortajada-Genaro, L. A.: Secondary organic aerosol formation from the photo-oxidation of benzene, Atmos. Environ., 47, 154-163, 10.1016/j.atmosenv.2011.11.020, 2012.

Carter, W. P. L., and Heo, G.: Development of revised SAPRC aromatics mechanisms, Atmos. Environ., 77, 404-414, 10.1016/j.atmosenv.2013.05.021, 2013.

Chen, J. Y., He, Z. G., Ji, Y. M., Li, G. Y., An, T. C., and Choi, W. Y.: (OH)-O-center dot radicals determined photocatalytic degradation mechanisms of gaseous styrene in TiO2 system under 254 nm versus 185 nm irradiation: Combined experimental and theoretical studies, Appl. Catal. B-Environ., 257, 117912, Unsp 11791210.1016/J.Apcatb.2019.117912, 2019.

Chen, J. Y., Yi, J. J., Ji, Y. M., Zhao, B. C., Ji, Y. P., Li, G. Y., and An, T. C.: Enhanced H-abstraction contribution for oxidation of xylenes via mineral particles: Implications for particulate matter formation and human health, Environ. Res., 186, 109568, Artn 10956810.1016/J.Envres.2020.109568, 2020.

Chen, Y., Tong, S. R., Wang, J., Peng, C., Ge, M. F., Xie, X. F., and Sun, J.: Effect of titanium dioxide on secondary organic aerosol formation, Environ. Sci. Technol., 52, 11612-11620, 10.1021/acs.est.8b02466, 2018.

Cocker III, D. R., Mader, B. T., Kalberer, M., Flagan, R. C., and Seinfeld, J. H.: The effect of water on gas–particle partitioning of secondary organic aerosol: II. m-xylene and 1,3,5-trimethylbenzene photooxidation systems, Atmos. Environ., 35, 6073-6085, 2001.

Doyle, G. J., Lloyd, A. C., Darnall, K. R., Winer, A. M., and Pitts Jr, J. N.: Gas phase kinetic study of relative rates of reaction of selected aromatic compounds with hydroxyl radicals in an environmental chamber, Environ. Sci. Technol., 9, 237-241, 1975.

Forstner, H. J. L., C, F. R., and Seinfeld, J. H.: Secondary organic aerosol from the photooxidation of aromatic hydrocarbons: molecular composition, Environ. Sci. Technol., 31, 1345-1358, 1997.

Geng, F., Tie, X., Xu, J., Zhou, G., Peng, L., Gao, W., Tang, X., and Zhao, C.: Characterizations of ozone, NOx, and VOCs measured in Shanghai, China, Atmos. Environ., 42, 6873-6883, 10.1016/j.atmosenv.2008.05.045, 2008.

Glasson, W. A., and Tuesday, C. S.: Hydrocarbon reactivities in the atmospheric photooxidation of nitric oxide, Environ. Sci. Technol., 4, 916-924, 1970.

Han, C., Liu, R., Luo, H., Li, G., Ma, S., Chen, J., and An, T.: Pollution profiles of volatile organic compounds from different urban functional areas in Guangzhou China based on GC/MS and PTR-TOF-MS: Atmospheric environmental implications, Atmos. Environ., 116843, 10.1016/j.atmosenv.2019.116843, 2019.

He, Z. G., Li, G. Y., Chen, J. Y., Huang, Y., An, T. C., and Zhang, C. S.: Pollution characteristics and health risk assessment of volatile organic compounds emitted from different plastic solid waste recycling workshops, Environ. Int., 77, 85-94, 10.1016/j.envint.2015.01.004, 2015.

Henze, D. K., Seinfeld, J. H., Ng, N. L., Kroll, J. H., Fu, T.-M., Jacob, D. J., and Heald, C. L.: Global modeling of secondary organic aerosol formation from aromatic hydrocarbons_ high- vs. low-yield pathways, Atmos. Chem. Phys., 8, 2405-2421, 2008.

Hu, D., Tolocka, M., Li, Q., and Kamens, R. M.: A kinetic mechanism for predicting secondary organic aerosol formation from toluene oxidation in the presence of NOx and natural sunlight, Atmos. Environ., 41, 6478-6496, 10.1016/j.atmosenv.2007.04.025, 2007.

Hu, L., Dylan B. Millet, Munkhbayar Baasandorj, Timothy J. Griffis, Katherine R. Travis, Christopher W. Tessum, Julian D. Marshall, Wesley F. Reinhart, Tomas Mikoviny, Markus Müller, Armin Wisthaler, Martin Graus, Carsten Warneke, and Joost de Gouw: Emissions of C6–C8 aromatic compounds in the United States_ Constraints from tall tower and aircraft measurements, J. Geophys. Res.: Atmos., 120, 826-842, 10.1002/, 2015.

Hurley, M. D., Sokolov, O., Wallington, T. J., Takekawa, H., Karasawa, M., Klotz, B., Barnes, I., and Becker, K. H.: Organic aerosol formation during the atmospheric degradation of toluene, Environ. Sci. Technol., 35, 1358-1366, 10.1021/es0013733, 2001.

Jang, M., and Kamens, R. M.: Characterization of Secondary Aerosol from the Photooxidation of Toluene in the Presence of NOx and 1-Propene, Environ. Sci. Technol., 35, 3626-3639, 10.1021/es010676+, 2001.

Ji, Y., Zhao, J., Terazono, H., Misawa, K., Levitt, N. P., Li, Y., Lin, Y., Peng, J., Wang, Y., Duan, L., Pan, B., Zhang, F., Feng, X., An, T., Marrero-Ortiz, W., Secrest, J., Zhang, A. L., Shibuya, K., Molina, M. J., and Zhang, R.: Reassessing the atmospheric oxidation mechanism of toluene, Proc. Natl. Acad. Sci. U S A, 114, 8169-8174, 10.1073/pnas.1705463114, 2017.

Ji, Y., Zheng, J., Qin, D., Li, Y., Gao, Y., Yao, M., Chen, X., Li, G., An, T., and Zhang, R.: OH-Initiated Oxidation of Acetylacetone: Implications for Ozone and Secondary Organic Aerosol Formation, Environ. Sci. Technol., 52, 11169-11177, 10.1021/acs.est.8b03972, 2018.

Jia, L., and Xu, Y.: Different roles of water in secondary organic aerosol formation from toluene and isoprene, Atmos. Chem. Phys., 18, 8137-8154, 10.5194/acp-18-8137-2018, 2018.

Johnson, D., Jenkin, M. E., Wirtz, K., and Martin-Reviejo, M.: Simulating the formation of secondary organic aerosol from the photooxidation of toluene, Environ. Chem., 2, 35-48, 10.1071/en04069, 2005.

Kalberer, M., Paulsen, D., Sax, M., Steinbacher, M., Dommen, J., Prevot, A. S. H., Fisseha, R., Weingartner, E., Frankevich, V., and Zenobi, R.: Identification of polymers as major components of atmospheric organic aerosols, Science, 303, 1659-1662, 2004.

Lane, T. E., Donahue, N. M., and Pandis, S. N.: Simulating secondary organic aerosol formation using the volatility basis-set approach in a chemical transport model, Atmos. Environ., 42, 7439-7451, 10.1016/j.atmosenv.2008.06.026, 2008.

Li, K., Chen, L., White, S. J., Yu, H., Wu, X., Gao, X., Azzi, M., and Cen, K.: Smog chamber study of the role of NH3 in new particle formation from photo-oxidation of aromatic hydrocarbons, Sci. Total Environ., 619-620, 927-937, 10.1016/j.scitotenv.2017.11.180, 2018.

Li, L., Tang, P., Nakao, S., Chen, C. L., and Cocker Iii, D. R.: Role of methyl group number on SOA formation from monocyclic aromatic hydrocarbons photooxidation under low-NOx conditions, Atmos. Chem. Phys., 16, 2255-2272, 10.5194/acp-16-2255-2016, 2016.

Li, Y., Lau, A. K. H., Fung, J. C. H., Zheng, J., and Liu, S.: Importance of NOx control for peak ozone reduction in the Pearl River Delta region, J. Geophys. Res.: Atmos., 118, 9428-9443, 10.1002/jgrd.50659, 2013.

Lim, Y. B., and Ziemann, P. J.: Effects of molecular structure on aerosol yields from OH radical-initiated reactions of linear, branched, and cyclic alkanes in the presence of NOx, Environ. Sci. Technol., 43, 2328-2334, 10.1021/es803389s, 2009.

Lindinger, W., Hansel, A., and Jordan, A.: Proton-transfer-reaction mass spectrometry (PTR–MS): on-line monitoring of volatile organic compounds at pptv levels, Chem. Soc. Rev., 27, 347-354, 1998.

Luo, H., Jia, L., Wan, Q., An, T., and Wang, Y.: Role of liquid water in the formation of O3 and SOA particles from 1,2,3-trimethylbenzene, Atmos. Environ., 217, 116955, https://doi.org/10.1016/j.atmosenv.2019.116955, 2019.

Luo, H., Li, G., Chen, J., Ma, S., Wang, Y., and An, T.: Spatial and temporal distribution characteristics and ozone formation potentials of volatile organic compounds from three typical functional areas in China, Environ. Res., 183, 109141, 2020a.

Luo, H., Li, G., Chen, J., Wang, Y., and An, T.: Reactor characterization and primary application of a state of art dual-reactor chamber in the investigation of atmospheric photochemical processes, J. Environ. Sci., 98, 161-168, 2020b.

Metzger, A., Dommen, J., Gaeggeler, K., Duplissy, J., Prevot, A. S. H., Kleffmann, J., Elshorbany, Y., Wisthaler, A., and Baltensperger, U.: Evaluation of 1,3,5 trimethylbenzene degradation in the detailed tropospheric chemistry mechanism, MCMv3.1, using environmental chamber data, Atmos. Chem. Phys., 8, 6453-6468, DOI 10.5194/acp-8-6453-2008, 2008.

Nakao, S., Clark, C., Tang, P., Sato, K., and Cocker Iii, D.: Secondary organic aerosol formation from phenolic compounds in the absence of NOx, Atmos. Chem. Phys., 11, 10649-10660, 10.5194/acp-11-10649-2011, 2011.

Nishino, N., Arey, J., and Atkinson, R.: Formation yields of glyoxal and methylglyoxal from the gas-phase OH radical-initiated reactions of toluene, xylenes, and trimethylbenzenes as a function of NO_2 concentration, J. Phys. Chem. A, 114, 10140-10147, 2010.

Odum, J. R., Hoffmann, T., Bowman, F., Collins, D., C, F. R., and Seinfeld, J. H.: Gas/particle partitioning and secondary organic aerosol yields, Environ. Sci. Technol., 30, 2580-2585, 1996.

Odum, J. R., Jungkamp, T. P., Griffin, R. J., Flagan, R. C., and Seinfeld, J. H.: The atmospheric aerosol-forming potential of whole gasoline vapor, Science, 276, 96-99, 1997.

Peng, J., Hu, M., Du, Z., Wang, Y., Zheng, J., Zhang, W., Yang, Y., Qin, Y., Zheng, R., Xiao, Y., Wu, Y., Lu, S., Wu, Z., Guo, S., Mao, H., and Shuai, S.: Gasoline aromatics: a critical determinant of urban secondary organic aerosol formation, Atmos. Chem. Phys., 17, 10743-10752, 10.5194/acp-17-10743-2017, 2017.

Sarrafzadeh, M., Wildt, J., Pullinen, I., Springer, M., Kleist, E., Tillmann, R., Schmitt, S. H., Wu, C., Mentel, T. F., Zhao, D., Hastie, D. R., and Kiendler-Scharr, A.: Impact of NOx and OH on secondary organic aerosol formation from β-pinene photooxidation, Atmos. Chem. Phys., 16, 11237-11248, 10.5194/acp-16-11237-2016, 2016.

Sato, K., Takami, A., Isozaki, T., Hikida, T., Shimono, A., and Imamura, T.: Mass spectrometric study of secondary organic aerosol formed from the photo-oxidation of aromatic hydrocarbons, Atmos. Environ., 44, 1080-1087, 10.1016/j.atmosenv.2009.12.013, 2010.

Sato, K., Takami, A., Kato, Y., Seta, T., Fujitani, Y., Hikida, T., Shimono, A., and Imamura, T.: AMS and LC/MS analyses of SOA from the photooxidation of benzene and 1,3,5-trimethylbenzene in the presence of NOx: effects of chemical structure on SOA aging, Atmos. Chem. Phys., 12, 4667-4682, 10.5194/acp-12-4667-2012, 2012.

Seinfeld, J. H.: Urban air pollution: State of the science, Science, 243, 745-752, 1989.

Song, C., Na, K., and Cocker, D. R., 3rd: Impact of the hydrocarbon to NOx ratio on secondary organic aerosol formation, Environ. Sci. Technol., 39, 3143-3149, 10.1021/es0493244, 2005.

Song, C., Na, K., Warren, B., Malloy, Q., and Cocker, D. R.: Secondary organic aerosol formation from the photooxidation of p- and o-xylene, Environ. Sci. Technol., 41, 7403-7408, 10.1021/es0621041, 2007.

Sun, J., Wang, Y., Wu, F., Tang, G., Wang, L., Wang, Y., and Yang, Y.: Vertical characteristics of VOCs in the lower troposphere over the North China Plain during pollution periods, Environ. Pollut., 236, 907-915, 10.1016/j.envpol.2017.10.051, 2018.

Tkacik, D. S., Presto, A. A., Donahue, N. M., and Robinson, A. L.: Secondary organic aerosol formation from intermediate-volatility

organic compounds: cyclic, linear, and branched alkanes, Environ. Sci. Technol., 46, 8773-8781, 10.1021/es301112c, 2012.

Tong, D., Chen, J. Y., Qin, D. D., Ji, Y. M., Li, G. Y., and An, T. C.: Mechanism of atmospheric organic amines reacted with ozone and implications for the formation of secondary organic aerosols, Sci. Total Environ., 737, 139830, ARTN 13983010.1016/j.scitotenv.2020.139830, 2020.

Volkamer, R., Platt, U., and Wirtz, K.: Primary and secondary glyoxal formation from aromatics: Experimental evidence for the bicycloalkyl-radical pathway from benzene, toluene, and p-xylene, J. Phys. Chem. A, 105, 7865-7874, DOI 10.1021/jp010152w, 2001.

Wang, W. G., Li, K., Zhou, L., Ge, M. F., Hou, S. Q., Tong, S. R., Mu, Y. J., and Jia, L.: Evaluation and Application of Dual-Reactor Chamber for Studying, Acta Phys. -Chim. Sin., 31(7), 1251-1259, 10.3866/PKU.WHXB201504161, 2015.

Wyche, K. P., Monks, P. S., Ellis, A. M., Cordell, R. L., Parker, A. E., Whyte, C., Metzger, A., Dommen, J., Duplissy, J., Prevot, A. S. H., Baltensperger, U., Rickard, A. R., and Wulfert, F.: Gas phase precursors to anthropogenic secondary organic aerosol: detailed observations of 1,3,5-trimethylbenzene photooxidation, Atmos. Chem. Phys., 9, 635-665, DOI 10.5194/acp-9-635-2009, 2009.

Xu, J., Griffin, R. J., Liu, Y., Nakao, S., and Cocker Iii, D. R.: Simulated impact of NOx on SOA formation from oxidation of toluene and m-xylene, Atmos. Environ., 101, 217-225, http://dx.doi.org/10.1016/j.atmosenv.2014.11.008, 2015.

Yang, Y., Vance, M., Tou, F., Tiwari, A., Liu, M., and Hochella, M. F.: Nanoparticles in road dust from impervious urban surfaces: distribution, identification, and environmental implications, Environ. Sci.: Nano, 3, 534-544, 10.1039/c6en00056h, 2016.

Zhao, D., Schmitt, S. H., Wang, M., Acir, I.-H., Tillmann, R., Tan, Z., Novelli, A., Fuchs, H., Pullinen, I., Wegener, R., Rohrer, F., Wildt, J., Kiendler-Scharr, A., Wahner, A., and Mentel, T. F.: Effects of NOx and SO_2 on the secondary organic aerosol formation from photooxidation of α-pinene and limonene, Atmos. Chem. Phys., 18, 1611-1628, 10.5194/acp-18-1611-2018, 2018.

Zhou, Y., Zhang, H., Parikh, H. M., Chen, E. H., Rattanavaraha, W., Rosen, E. P., Wang, W., and Kamens, R. M.: Secondary organic aerosol formation from xylenes and mixtures of toluene and xylenes in an atmospheric urban hydrocarbon mixture: Water and particle seed effects (II), Atmos. Environ., 45, 3882-3890, 10.1016/j.atmosenv.2010.12.048, 2011.

Ziemann, P. J.: Effects of molecular structure on the chemistry of aerosol formation from the OH-radical-initiated oxidation of alkanes and alkenes, Int. Rev. Phys. Chem., 30, 161-195, 10.1080/0144235x.2010.550728, 2011.

Zou, Y., Deng, X. J., Zhu, D., Gong, D. C., Wang, H., Li, F., Tan, H. B., Deng, T., Mai, B. R., Liu, X. T., and Wang, B. G.: Characteristics of 1 year of observational data of VOCs, NOx and O3 at a suburban site in Guangzhou, China, Atmos. Chem. Phys., 15, 6625-6636, 10.5194/acp-15-6625-2015, 2015.

Table 1. Fitting yield curve parameters of two-product semi-empirical models.

AHs	α_1	$K_{om,1}$ (m^3 μg^{-1})	α_2	$K_{om,2}$ (m^3 μg^{-1})
Benzene	0.341	0.022	0.242	0.005
Toluene	0.157	0.027	0.162	0.005
Ethylbenzene	0.285	0.023	0.422	0.005
m-xylene	0.103	0.057	0.086	0.005
o-xylene	0.345	0.024	0.017	0.005
p-xylene	0.085	0.074	0.057	0.005
123-TMB	0.114	0.025	0.082	0.005
124-TMB	0.068	0.075	0.080	0.005
135-TMB	0.080	0.085	0.032	0.005

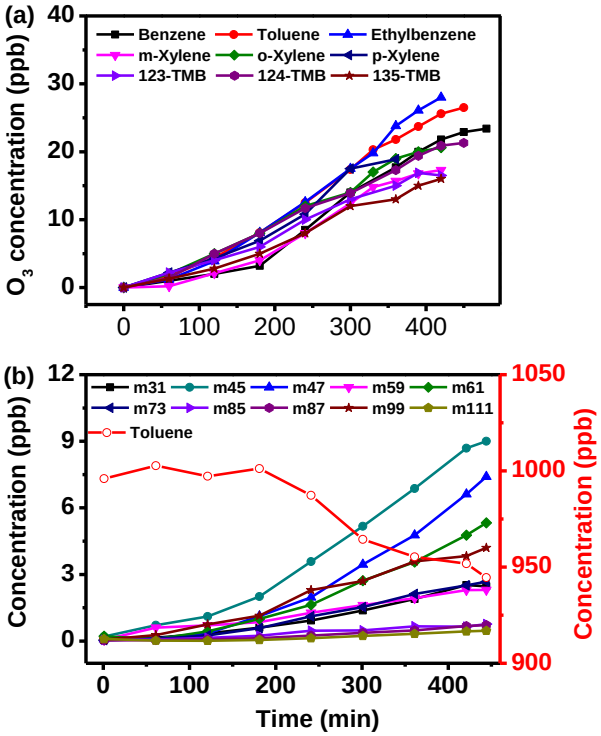

460 **Figure 1. (a) O_3 formation curve from AH photochemical oxidation (2110 ppb of benzene, 996 ppb of toluene, 1060 ppb of ethylbenzene, 889 ppb of m-xylene, 1160 ppb of o-xylene, 1040 ppb of p-xylene, 824 ppb of 123-TMB, 935 ppb of 124-TMB, 913 ppb of 135-TMB) without NO_x. (b) The concentration variation of intermediates formed from 996 ppb of toluene photochemical oxidation without NO_x.**

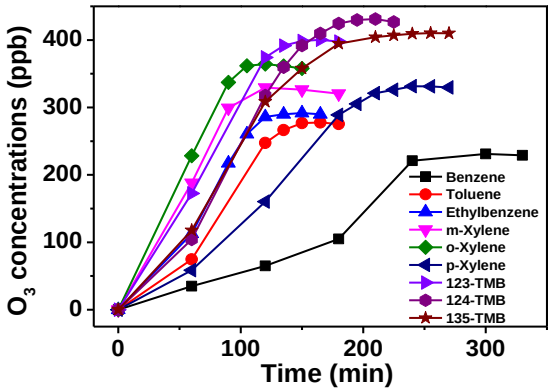

Figure 2. O_3 formation curve from AH photochemical oxidation with the presence of NO_x (2000 ppb of benzene and 160.2 ppb of NO_x, 1048 ppb of toluene and 162.0 ppb of NO_x, 1050 ppb of ethylbenzene and 162.4 ppb of NO_x, 889 ppb of m-xylene and 172.1 ppb of NO_x, 1052 ppb of o-xylene and 159.8 ppb of NO_x, 1040 ppb of p-xylene and 157.2 ppb of NO_x, 956 ppb of 123-TMB and 171.4 ppb of NO_x, 1010 ppb of 124-TMB and 169.5 ppb of NO_x, 1040 ppb of 135-TMB and 164.2 ppb of NO_x).

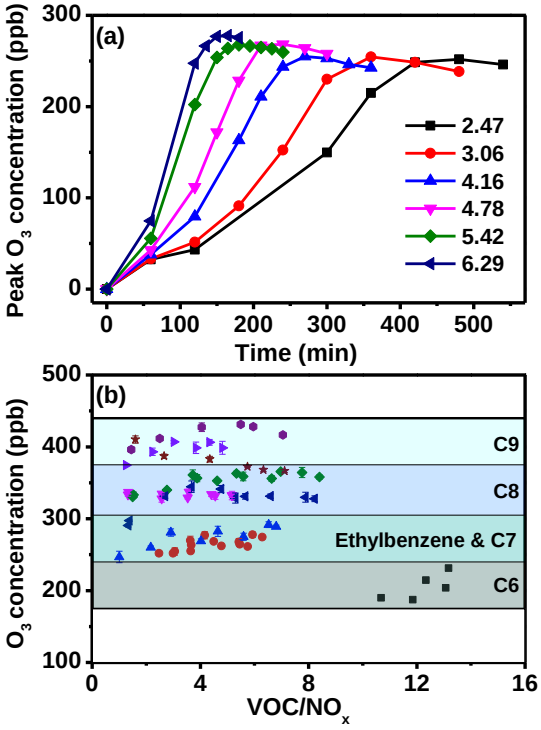

Figure 3. (a) O_3 formation curve of toluene photochemical oxidation at different VOC/NO_x ratio and (b) change trend of the peak O_3 generated by photochemical oxidation of AHs at different VOC/NO_x ratio (square: benzene; circle: toluene; upper triangle: ethylbenzene; lower triangle: m-xylene; diamond: o-xylene; left triangle: p-xylene; right triangle: 123-TMB; hexagon: 124-TMB; pentacle: 135-TMB).

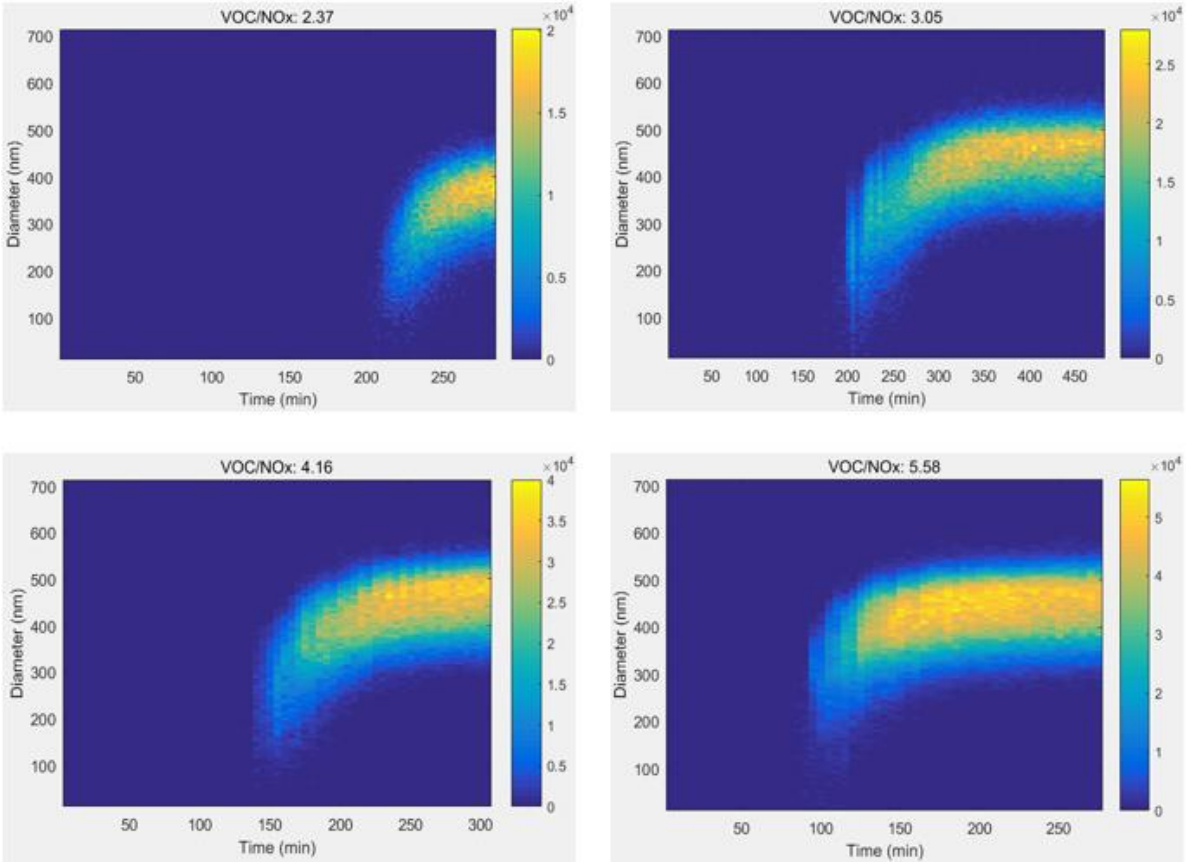

Figure 4. Nanoparticle distribution from toluene photochemical oxidation varied with time at different VOC/NO_x ratio (the initial concentrations of NO_x were in the range of 158.2 to 179.7 ppb).

480

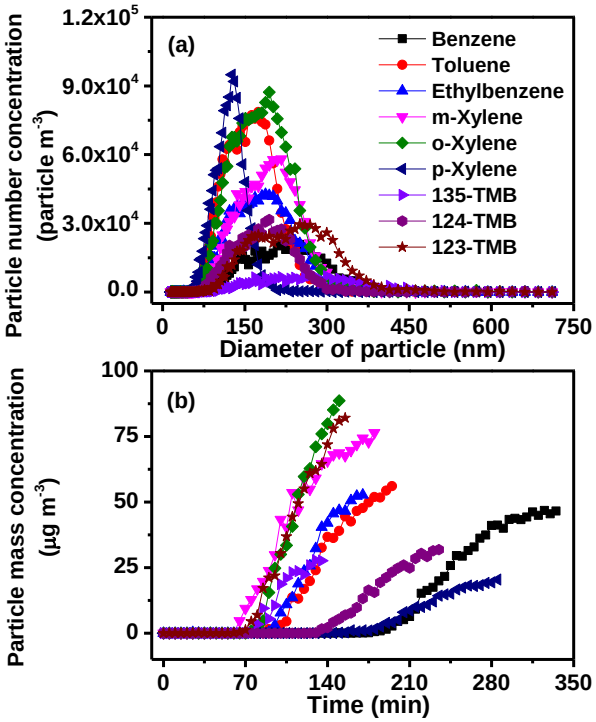

Figure 5. (a) Number concentration and (b) mass concentration of SOA produced from AH photochemical oxidation with the presence of NO_x (2000 ppb of benzene and 160.2 ppb of NO_x, 1048 ppb of toluene and 162.0 ppb of NO_x, 1050 ppb of ethylbenzene and 162.4 ppb of NO_x, 889 ppb of m-xylene and 172.1 ppb of NO_x, 1052 ppb of o-xylene and 159.8 ppb of NO_x, 1040 ppb of p-xylene and 157.2 ppb of NO_x, 956 ppb of 123-TMB and 171.4 ppb of NO_x, 1010 ppb of 124-TMB and 169.5 ppb of NO_x, 1040 ppb of 135-TMB and 164.2 ppb of NO_x).

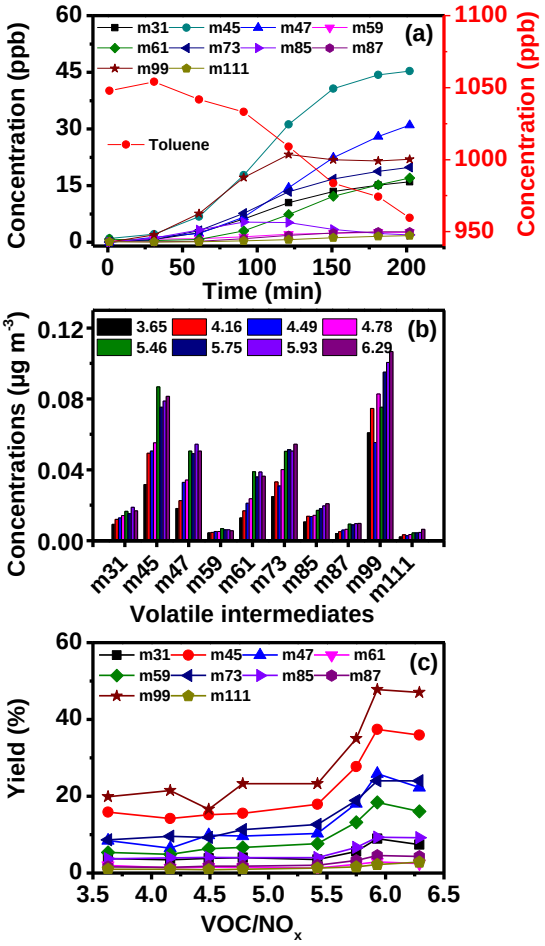

Figure 6. Intermediates formed from toluene photochemical oxidation in the presence of NO_x (a) concentration variation with the reaction time (1048 ppb of toluene and 162.0 ppb of NO_x) (b) concentration and (c) yield with the increase of VOC/NO_x ratio.

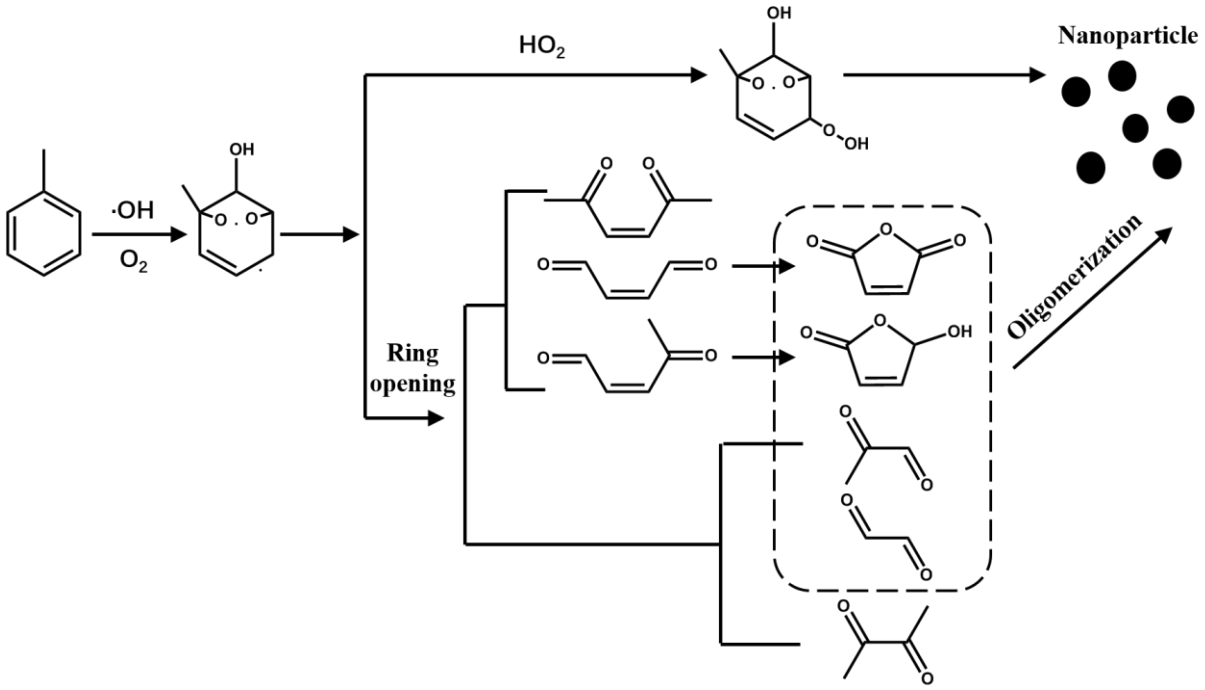

Figure 7. The possible photochemical oxidation mechanism of toluene to SOA formation.